Experimental Characterization of Actuators for Micro Air Vehicles

Giorgio Guglieri[a] and Daniele Sartori[b]
[a]Associate Professor, Politecnico di Torino Dipartimento di Ingegneria Aeronautica e Spaziale
Torino, Italy
Email: giorgio.guglieri@polito.it

[b]PhD Student, Politecnico di Torino Dipartimento di Ingegneria Aeronautica e Spaziale
Torino, Italy
Email: daniele.sartori@polito.it

Received on 28 February 2011; Accepted on 30 June 2011

ABSTRACT

Mini-UAVs and RC slow flyers require compact, lightweight and responsive actuators. Shape memory alloy wires can be used to design ultra-light micro-servos. This technology relies on the reversible change in crystalline structure that a SMA wire undergoes when electricity runs through it. The resulting contraction is used to deflect the aircraft control surfaces. This paper introduces SMA wires technology and its application to the design of a small-size and light-weight actuator for elevon type controls. A conventional servo is taken as a reference to compare static and dynamic performance of the realized wire configuration prototype. A wind tunnel experiment is set up to test the behavior at different airspeeds and the servos response to variable frequency input is recorded. Extensive data analysis is performed to estimate the system models and to predict their bandwidth. In particular, Prediction-Error Minimization method is applied and Akaike's Final Prediction-Error is used to evaluate the model fitting accuracy. Results show that the SMA servo, despite its excellent general characteristics (i.e. small size, light weight, high power to weight ratio, silent operation, long life) seems to be only partially suitable for small scale flying vehicles due to its low bandwidth. By contrast, the conventional low cost servo provides a faster response in terms of torque output but fails to be accurate and repeatable under dynamic load conditions.

Nomenclature

b	wing span (wing)	c_f	elevon chord (wing)
c	mean aerodynamic chord (wing)	D	diameter (wire)
C_H	hinge moment coefficient	f_t	thermal cycle rate (wire)
FPE	Final Prediction-Error	SMA	Shape Memory Alloy
H	hinge moment (wing)	τ	trailing edge angle (wing)
I	current (wire)	t	thickness (wing)
P	power (wire)	t_C	contraction time (wire)
PEM	Prediction-Error Minimization	t_E	extension time (wire)
R	resistivity (wire)	UAV	Unmanned Aerial Vehicle
RC	Radio Controlled	V	airspeed
ρ	air density	ω_n	bandwidth
S_f	elevon surface (wing)		

1. INTRODUCTION

Actuators are like the muscles of a mechanical system, the parts which convert stored energy into movement. As an example, actuators are electric motors that spin a wheel or gear, or linear actuators that control industrial robots in factories.

Fixed wing remotely controlled slow flyers (Fig.1) and mini-UAVs (Fig.2) are typically controlled by the deflection of control surfaces (Fig.3). Slow flyers and park flyers are very light recreational radio controlled models used for close range indoor and sometime outdoor flight, designed to be extremely light so that the stall speed is minimized.These fun flyers normally exhibit powered flight as propeller thrust compensates for the degraded lifting capabilities of lifting surfaces (i.e. very low dynamic pressure).

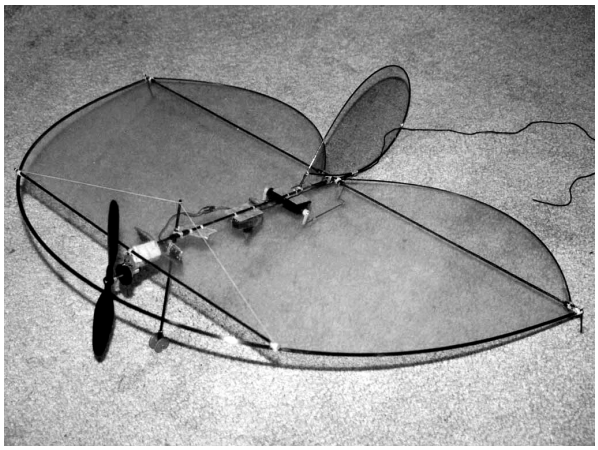

Figure 1: An example of RC model (slow flyer).

Figure 2: An example of a mini-UAV (hand launch of MAVTech MH850).

Micro and mini-UAVs are very compact semi-autonomous flying robots mainly exploiting a fixed wing configuration even if rotary and flapping wing concepts were also implemented. The purpose of their missions (either civil or military) is the surveillance of confined space. An extensive outline of the evolution of these flying platforms is given in Ref.[1][2]. The actuators for these applications evolved consistently during last years, increasing their performances, becoming lighter, more compact and responsive to wider bandwidth inputs.

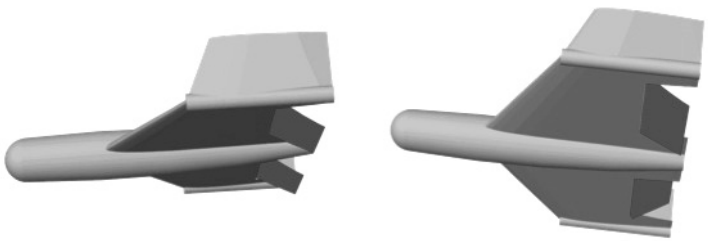

Figure 3: The trailing edge control surfaces (elevon modes).

Servo actuators used to operate radio controlled model aircraft, boats, and other gadgets are easily available from commercial distributors. These are small boxes that contain: a DC electric motor, gears with an output shaft, a position-sensing mechanism, and a control circuitry. There are numerous types of servos. They differ in weight, precision, speed, and strength -all of which are reflected in price. Most servos require a power supply between 4.8 V and 6.0 V. The higher the voltage, the faster the servo will move and the more torque it will have.

A standard RC radio receiver sends Pulse Width Modulation (PWM) signals to the servo. The electronics inside the servo translate the width of the pulse into a position. When the servo is commanded to rotate, the motor is powered until the potentiometer reaches the value corresponding to the commanded position. The length of the pulse indicates the position to take. Nominally, when the pulse width is 0.6-2.4 ms the servo angular position is ∓ 45 deg. A pulse width of 1.5 ms sets the servo to central position. Increasing the pulse width by 10 µs results in about a degree of movement on the output shaft. The servo is usually controlled by three wires: ground, power, and control. The servo will move based on the pulses sent over the control wire, which set the angle of the actuator arm. The servo expects a pulse every 20 ms in order to gain correct information about the angle.

Some recent advances in alternative types of actuators, powered by electricity, are based on muscle wires also known as shape memory alloys or Flexinol wires. These materials contract slightly (typically under 5%) when electricity runs through them. Muscle wire is a registered trademark of Mondotronics Inc. [3] and Flexinol is a trademark of Dynalloy Inc. [4]. These Nickel-Titanium alloys are manufactured as small wires (see Fig.4) under the trade name of Flexinol to differentiate them from other shape memory alloys which do not have these same properties. The physical properties of Flexinol [5] are summarized in Tab.1. Actuator wires contract much like little muscles a distance of approximately 3-5% when they are "on" and relax when they are "off".

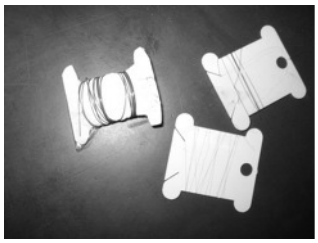

Figure 4: The shape memory alloy (Flexinol wire).

Table 1. The characteristics of Flexinol wires.

D (μm)	25	37	50	100	150	250
R (Ω/m)	1770	860	510	150	50	20
I (mA)	20	30	50	180	400	1000
P (W/m)	0.71	0.78	1.28	4.86	8	20
t_C (s)	0.1	0.1	0.1	0.1	0.1	0.1
t_E (s)	1.0	1.1	1.2	1.7	2.9	6.6
f_t (Hz)	0.92	0.87	0.77	0.55	0.34	0.15

The thermal shape memory effect [6] is caused by the changes of crystalline structure from a highly symmetrical structure (austenite) to a structure with a less symmetrical crystalline organization (martensite). SMAs can be plastically deformed at low temperature and upon exposure to higher temperature, return to the shape prior to the deformation. When cooled below the transformation temperature, the SMA transforms to its martensitic phase, enabling easy deformation, while when reheated above the transformation temperature, it will resume its memorized austenitic shape. The process is fully reversible. The phase transformation shows hysteresis in the strain-temperature, stress-strain and stress-temperature relations (see Tab.1). The Young's modulus and the electrical resistivity change drastically during transformation. The activation of Flexinol starts from 68^oC to 78^oC while the relaxation starts at 52^oC and finishes at 42^oC. The maximum strength under working load is 600 MPa even if a nominal condition set for 190 MPa is suggested. A minimum load is required (35 MPa) as pre-

tensioning of the wire actuator is usually obtained with some type of restoring action (bias spring).

Simulation models were also developed to predict the actual behavior of SMA-based actuators [7, 8, 9].

Muscle wires have been extensively used for robotics and bio-medical applications [6, 10, 11, 12, 13]. The advantages of these actuators are: small size, light weight, high power to weight ratio, smooth and silent operation, long life, benefit for miniaturization and precise controllability. The low operating frequency due to the limited cooling rate, the restricted energy effciency due to the conversion of heat into mechanical energy, the nonlinear properties, degradation and fatigue, the need for smooth bending and shaping in coils or loops without sharp edges are their disadvantages. Actuator wires have been also applied to deflect the control surfaces of slow flying remotely controlled aircraft for recreational use [14, 15]. More recently, a lightweight servo, based on contractile BioMetal Fiber, was customized for very light RC aircraft model sizes [16].

2. PRESENT WORK

The purpose of the present work is:

1. to design an ultra-light micro wire actuator for elevon type controls, without push-rods and leverages, operating with low currents and compatible with 4.8-6 V supplies, controlled with the same circuit adopted for conventional servos;
2. to compare the wind-off and wind-on performances of the wire actuator with a conventional RC servo;
3. to asses the frequency domain response of conventional and wire actuators in different operating conditions (these last data are vital for realistic flight simulation).

3. THE EXPERIMENTAL SETUP

Two types of actuators (see Fig.5) are compared in the present experimental activity. The first servo is a conventional analog sub-micro servo produced by GWS (see Tab.2). The second servo is assembled using two Flexinol wires (diameter 50 μm) installed as double loop triangle actuators working on opposite sides of the elevator. When a filament is powered, its contraction is partially balanced by the opposite inactive filament that acts as a coupled restoring spring. The diameter of wire was selected as a compromise between acceptable cycle rates (bandwidth) and adequate torque output on the control surface. A tensioning screw was used on one end of the wire loop to trim and pre-load the actuator. An attempt to design high-torque multi-wire actuators was abandoned due to the unacceptable levels of wire to wire friction. As a matter of fact, the minimization of friction is a major concern for the design of this type of wire actuators. A servo amplifier for magnetic-coil actuators was used to power and control the muscle wires. More specifically, a circuit board from a GWS IQ-100 servo is used, replacing the internal potentiometer with two 2.2 kΩ resistors (see Fig.6). A lightweight plastic support is machined and it fits inside the elevator replacing one of the deflection hinges of the control surface. The overall weight of the SMA servo including wires, support hinge and circuit is 0.025 N. Voltage supply is set through a stabilized source at 6 V for both actuators.

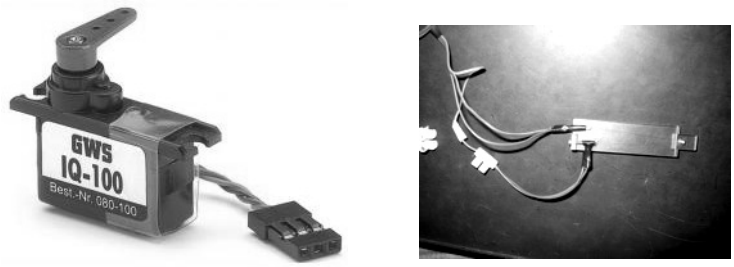

Figure 5: The conventional servo and the shape memory alloy actuator.

Table 2. The characteristics of the conventional servo.

Model	GWS IQ-100 analog sub-micro
Torque	0.084 Nm (@ 6 V)
Time response (60 deg)	0.09 s (@ 6 V)
Weight	0.054 N
Construction	No bearings - Plastic gears

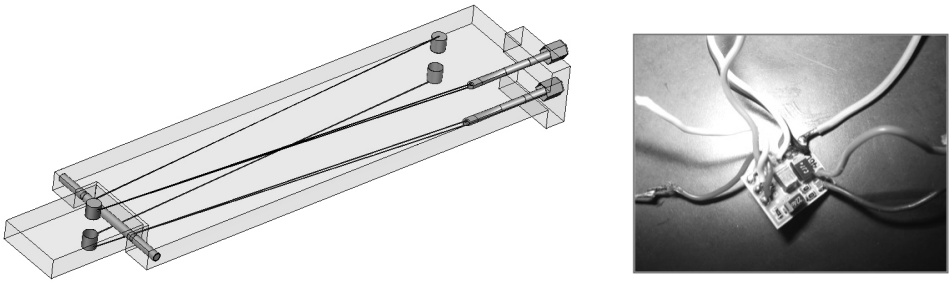

Figure 6: The components of the shape memory alloy actuator.

The servos are installed on a rectangular wing (chord c = 180 mm and span b = 300 mm). The material chosen for the construction of the wing is Expanded Poly Propylene, a synthetic foam. This material is extremely light and very tough, it doesn't absorb moisture and it has good surface finish. Forming is by simple hot wire cutting, a low cost manufacturing process. The airfoil selected is symmetric (NACA 0009) with a thickness t/c = 0.09. Two separate elevons (see Fig.7) are obtained (elevon chord c_f = 30 mm and flap-chord ratio c_f /c = 0.165), each deflected by a separate servo. An external push-rod is required for the conventional servo. Due to the low aspect ratio of the wing planform, two circular endplates are also added to provide a uniform lift distribution along the span.

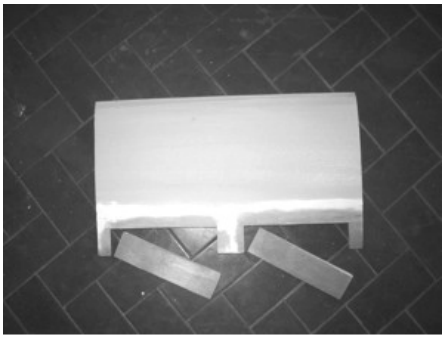

Figure 7: The experimental model (wing planform).

The hinge moments were estimated to verify that both servo actuators were operated within compatible ranges. The aerodynamic hinge moment H_a can be modeled as

$$H_a = \frac{1}{2} \cdot C_H \cdot \rho \cdot V^2 \cdot S_f \cdot c_f. \tag{1}$$

C_H is the hinge moment coeffcient, ρ is the air density, V is the airspeed, S_f and c_f are respectively elevon surface and chord. The hinge moment coeffcient for a symmetric airfoil is represented by

$$C_H = b_1 \cdot \alpha + b_2 \cdot \delta. \tag{2}$$

The parameters b_1 and b_2 are estimated through a graphical procedure [17], they depend on

flap-chord ratio c_f/c, airfoil thickness t/c and trailing edge angle τ =15 deg.

A 50% stick deflection was considered (±20 deg) at zero lift condition. The maximum aerodynamic hinge moment is H_a = 0.003 Nm evaluated for an airspeed of 10 m/s, a typical flight condition for a slow flying vehicle. The magnitude of output torque for the conventional servo (see Tab.2) is suffcient to compensate the aerodynamic load on the elevator. For the wire actuator, an offset due to the bias spring effect H_s = 0.004 Nm is added obtaining the total hinge moment as $H = H_a + H_s$ = 0.007 Nm. The SMA servo (wire diameter 50 μm) can provide a maximum torque output H = 0.016 Nm and a nominal torque output H = 0.005 Nm, assuming a force displacement of 3.5 mm (gear ratio is 70%) and 4 parallel wires with a single active length of 70 mm. The torque output is exceeding the nominal operating conditions. Hence, a maximum wind tunnel airspeed of 7.5 m/s is selected.

The wing is installed on a mechanical support (see Fig.8). The angle of attack of the airfoil can be changed rotating the wing tip pins suspended with bearings. The incidence is set to zero for the current experiments.

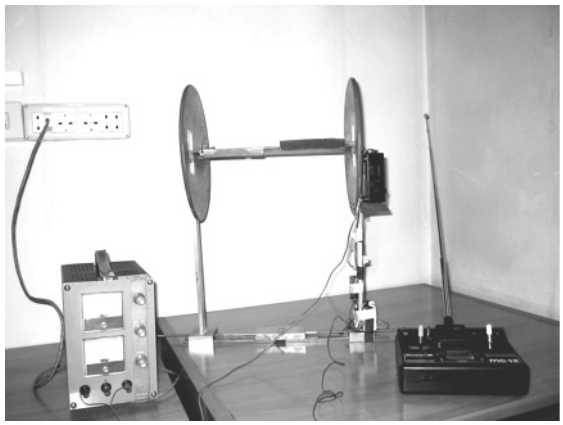

Figure 8: The experimental setup.

The servo displacement is controlled through a radio link. When the operator acts on the stick of the remote control the receiver installed on the model wing drives the servo acting on the elevon. The pulse width of the control signal is replicated by a digital servo tester. The motion of the control surface is tracked by an external digital video camera without aerodynamic or mechanical interference with the experimental setup installed in the test section. The video sequence is elaborated later (decomposition into video frame sequence). A set of optical markers is used as a cross-check of the angular displacement of the servo.

The experimental tests have been carried out in the Small Wind Tunnel (SWT) at the Aerospace Engineering Department of Politecnico di Torino (see Fig.9). It is an open circuit wind tunnel with a square test section (0.9 m x 0.9 m) and circular flow field (diameter 0.4 m x length 0.73 m). The indraft wind tunnel used has a honeycomb and two inlet screens for turbulence reduction, followed by an entrance cone characterized by a 3.5:1 contraction ratio. The maximum power is 7.5 kW and acceptable flow quality is granted (turbulence level below 0.5%) in the speed range of approximately 2.5-25 m/s.

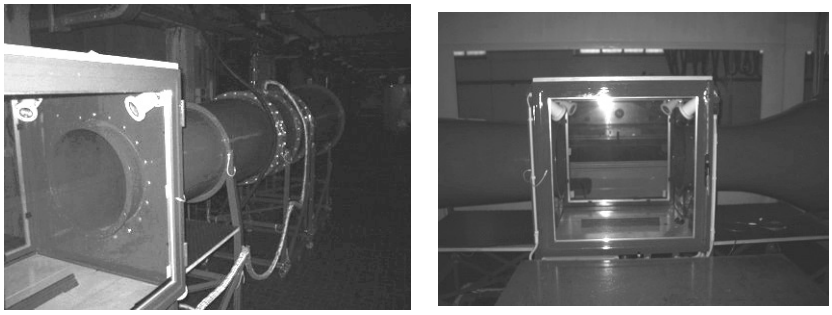

Figure 9: The experimental facility (SWT).

4. THE EXPERIMENTAL RESULTS

Conventional and SMA servos are tested at four different airspeeds: 0, 2.5, 5 and 7.5 m/s. Large frequency sweeps ranging from 0.1 to 4 Hz over a time interval up to 150 s are sent as input to the servos (approximately 50% of full stick range). The decomposition of the video sequence recorded at 25 Hz (the sampling time interval is 0.04 s) allows storing a time domain input and output series of points (see Fig.10). The analysis of these data is carried out in order to identify the bandwidth of the system ω_n.

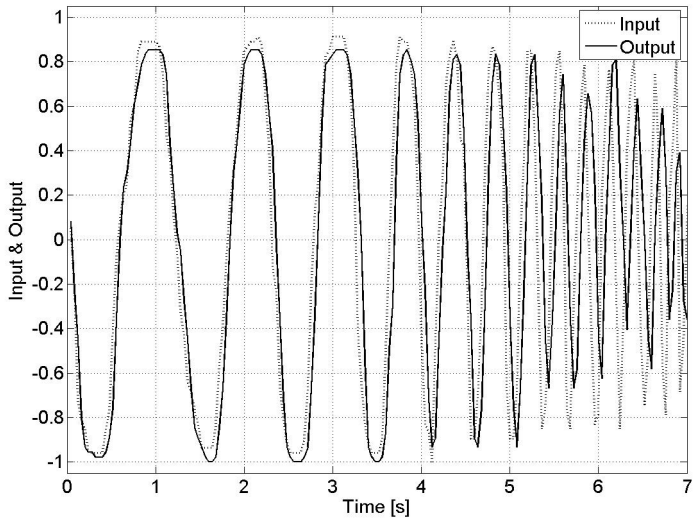

(a) Traditional servo

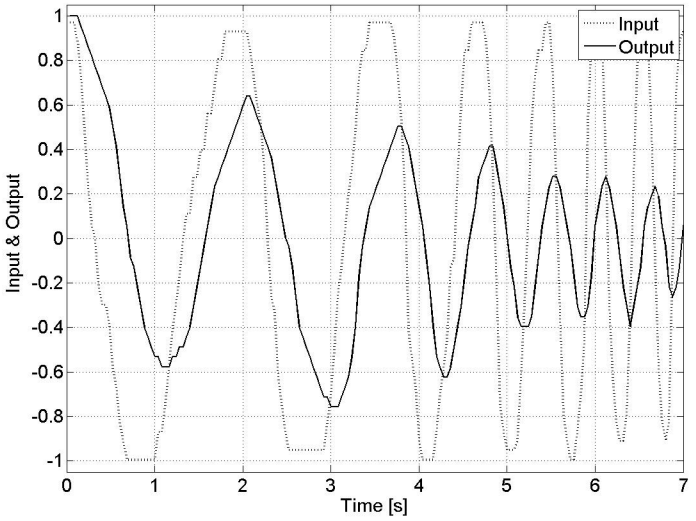

(b) Shape memory alloy servo

Figure 10: Example of time domain normalized input and output series for V = 5 m/s.

For a first order system, as servos are assumed to behave (higher order approximations do not match the experimental outputs of the SMA servo), the parameter ω_n represents the condition where attenuation filters the pilot inputs and phase lags 45 deg. This is the threshold for the pilot anticipation response, as for higher attenuation and phase delays the pilot can hardly anticipate the system reactions. A servo with high ω_n allows quick pilot reactions, the upper limit being imposed by human response capabilities, estimated in 2-4 Hz. The experimental time series are elaborated with a high level software environment to estimate the system model parameters. The selected approach relies on the Prediction-Error Minimization Method (PEM). This algorithm minimizes the error generated from an optimally

determined predictor [18]. In this case the error is minimized through the scalar cost function:

$$V_N(G,H) = \sum_{t=1}^{N} e^2(t) \tag{3}$$

where e is the error for a linear model calculated subtracting the predicted output $G(z)u(t)$ to the measured output:

$$e(t) = H^{-1}(z) \cdot [y(t) - G(z)u(t)] \tag{4}$$

Note that z is the discrete variable, $G(z)$ and $H(z)$ are the transfer functions of the estimator, $u(t)$ is the input and $y(t)$ is the measured output. The first order state space model ($x(t)$ is the state variable, A, B, C, D are the state matrices and K is the output error model matrix)

$$x(t+T_S) = Ax(t) + Bu(t) + Ke(t) \tag{5}$$

$$y(t) = Cx(t) + Du(t) + e(t) \tag{6}$$

which fits the experimental data is estimated and the related continuous time transfer function is easily computable. Figure 11 shows the PEM transfer function estimation compared to the empirical transfer function computed as the ratio of the output Fourier transform to the input Fourier transform of the experimental data.

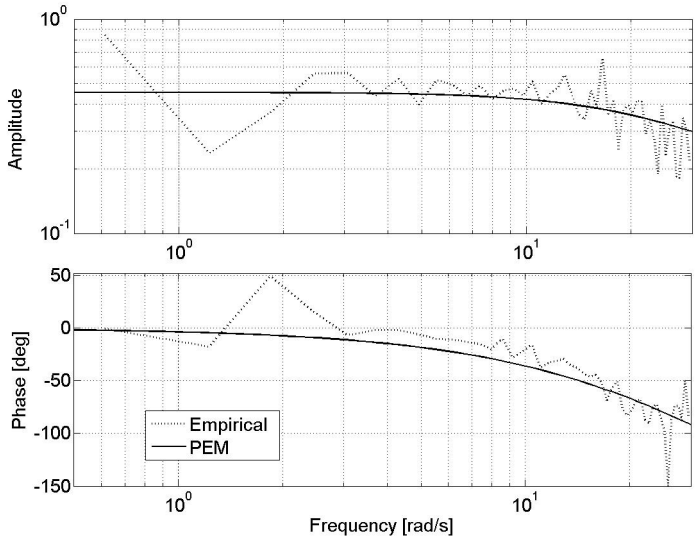

(a) Traditional servo

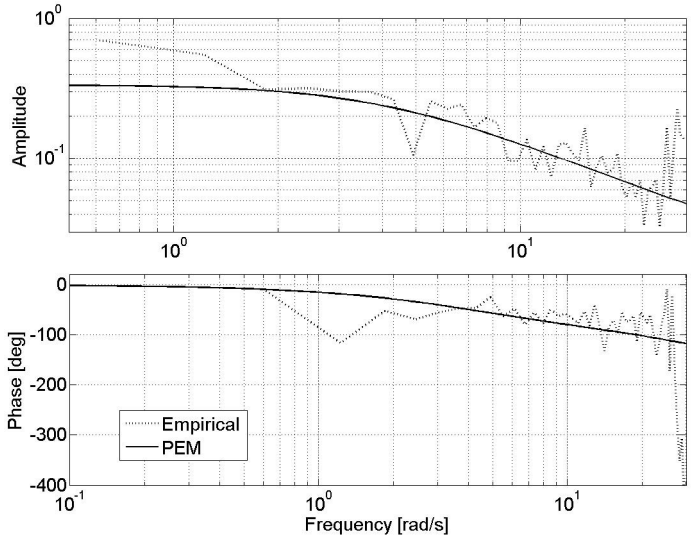

(b) Shape memory alloy servo

Figure 11: Example of transfer function estimate for $V = 5$ m/s.

In order to reduce the noise influence on the model, a first order Butterworth lowpass filter is applied to the data with a cut off frequency equal to half the Nyquist frequency. The corresponding bandwidth for both conventional and SMA servos are listed in Tab.3.

Table 3. Bandwidth ω_n of conventional and SMA servos.

Airspeed (m/s)	Conventional (Hz)	SMA (Hz)
0	1.574	0.251
2.5	3.452	0.579
5	3.752	0.644
7.5	3.669	0.934

It is possible to observe for both servo types an increase of bandwidth with airspeed. In fact, the rise of the aerodynamic force, and so of the hinge moment, acts as an increase of the restoring actions in the system. The wire actuator is also influenced by the acceleration of the extension phase produced by cooling effect of the airflow (as in the real flight case). Nevertheless, SMA servos show a lower bandwidth throughout all the speed range and their performance is dramatically poorer at the lower end where slow flyers and mini-UAVs are expected to fly.

The analysis of the results shows that the SMA servo exhibits a lower responsiveness with a limited ability to follow complex commands with an extended frequency content. Furthermore the gain drops as airspeed increases (not shown here) due to the torque output limitations of the double wire layout adopted for this experiment. Attempts to use multi-wire solutions were in any case in effective as a consequence of wire-to-wire friction penalties. In any case, the servo range normally used during non aggressive flight is quite limited and the loss of effectiveness may be compensated by a larger stick action from the pilot. As an alternative, SMA servo may also find its application in secondary control surfaces such as redundant rudders or spoilers. Here slower time responses and smaller torque outputs are acceptable, its lower weight (0.025 N instead of 0.054 N of the conventional servo) represents a substantial asset. This trade-off can hardly be accepted for primary control surfaces where a quick command response (high ω_n) is necessary. For this application the conventional servo, that deprived of its plastic case can benefit a considerable weight loss (up to 40%), is thus preferred.

Another effect of airspeed is the thermal drift of the test section that alters the state of the wire actuator i.e. the transition phases and the duration of contraction/extension intervals. Some warm-up may be required to minimize this undesired collateral effect.

Direct measurement of current was not possible without interference with the control circuit board driving the servo displacement. Only the current offset between the two types of servos could be measured under working conditions, demonstrating that the driving current of the conventional actuator is higher (ΔI = 100 mA).

The Akaike's Final Prediction-Error scaled as a percentage of the averaged output is used [19] to evaluate the model fitting accuracy (see Tab.4). This algorithm tests the model with different sets of input data. FPE is defined as:

$$FPE = R \cdot ((1 + (M + 1)N)/(1 - (M + 1)N)) \tag{7}$$

where M is the order of the auto-regressive model, R is the mean square of the residuals and N is the length of the data record.

The conventional servo shows a degradation of model compliance (first order type response) as the airspeed increases. This is the result of the mechanical inaccuracies of the internal plastic gears and of external push-rod enhanced by the aerodynamic loads acting on the elevon, mainly in the higher frequency range. The analysis of the data shows that the standard servo is tracking accurately the stick input sweeps below 1 Hz (as confirmed by Fig.10). The wind-off (i.e. no airspeed) prediction error (approximately 5% for both servo types) is a guess of the discrepancy between model fit and measurements deriving from modeling-experimental errors and servo bias.

Table 4. Prediction error for conventional and SMA servos.

Airspeed (m/s)	Conventional (%)	SMA (%)
0	6.5	5.0
2.5	24.0	5.3
5	23.7	4.0
7.5	27.1	2.4

5. CONCLUSIONS

Results show that SMA servo, despite its excellent general characteristics (i.e. small size, light weight, high power to weight ratio, silent operation, long life) seems to be only partially suitable for small scale flying vehicles due to its low bandwidth and the limited torque output. Thermal sensitivity may be a precluding factor for outdoor application of SMA servos. By contrast, the low cost conventional servo provides a faster response in terms of torque output but fails to be accurate and repeatable under higher frequency dynamic load conditions. Part of this inaccuracy also derives from its installation (push-rod and other mechanical offsets). Finally, these experimental results provide a reference for simulation models of slow flyers and mini-UAVs including actuators and bandwidth-dependent delays.

ACKNOWLEDGMENTS

The authors wish to acknowledge the invaluable technical assistance given by Mr. Ezio Dadone.

REFERENCES

[1] Müller, T.M., "Fixed and Flapping Wing Aerodynamics for Micro Air Vehicle Applications", AIAA Progress in Astronautics and Aeronautics Series, 2001.

[2] Müller, T.M., Kellogg, T.J., Ifju, P.G., Shkarayev, S.V., "Introduction to the Design of Fixed-Wing Micro Air Vehicles", AIAA Education Series, 2007.

[3] http://www.jameco.com/

[4] http://www.dynalloy.com/

[5] Gilbertson, R.G., "Muscle Wires Project Book", Mondo-Tronics Inc., 2000.

[6] Mandru, D., Lungu, I., Noveanu, S., Tatar, O., "Shape Memory Alloy Wires as Actuators for a Minirobot", IEEE International Conference on Automation Quality and Testing Robotics, 2010.

[7] Huang, W., "On the Selection of Shape Memory Alloys for Actuators", Materials and Design, 2002, 23, 11-19.

[8] Dutta, S.M., Ghorbel, F.H., "Differential Hysteresis Modeling of a Shape Memory Alloy Wire Actuator", IEEE/ASME Transactions on Mechatronics, 2005, 10(2), 189-197.

[9] Dabney, J.B., Dutta, S.M., Ghorbel, F.H., "Modeling and Control of a Shape Memory Alloy Actuator", Pro-ceedings of the 2005 IEEE International Symposium on Intelligent Control, Limassol, Cyprus, 2005.

[10] Sreekumar, M., Nagarajan, T., Singaperumal, M., "Critical Review of Current Trends in Shape Memory Alloy Actuators for Intelligent Robots", Industrial Robot: An International Journal, 2007, 34(4), 285-294.

[11] Song, G., "Design and Control of a Nitinol Wire Actuated Rotary Servo", Smart Materials and Structures, 2007, 16, 1796-1801.

[12] Kitamasu, M., Yoshida, M., "Basic Study for New Type Actuator Using Shape Memory Alloy", 23rd Annual EMBS International Conference, Istanbul, Turkey, 2001.

[13] Dutta, T., Chau, T., "A Feasibility Study of Flexinol as the Primary Actuator in a Prosthetic Hand", Canadian Conference on Electrical and Computer Engineering, Toronto, Canada, 2003.

[14] Keennon, M., "Muscle Wire Basics", Radio Control Microflight, June 2002.

[15] Keennon. M., "Build a Muscle-Wire Actuator", Radio Control Microflight, June 2002.

[16] http://www.toki.co.jp/

[17] Etkin, B., Reid, L.D., "Dynamics of Flight: Stability and Control", Wiley, 1995.

[18] Ljung, L., "System Identification: Theory for the User", Prentice-Hall, 1999.

[19] Akaike, H., "Fitting autoregressive models for prediction", Annals of the Institute of Statistical Mathematics, 1969, 21, 243-247.